Case Studies in Thermal Engineering 45 (2023) 102959

Contents lists available at ScienceDirect

Case Studies in Thermal Engineering

journal homepage: www.elsevier.com/locate/csite

Computational study of Cattaneo–Christov heat flux on cylindrical surfaces using CNT hybrid nanofluids: A solar-powered ship implementation

A.M. Obalalu [a], S.O. Salawu [b], M. Asif Memon [c], O.A. Olayemi [d], Mohamed R. Ali [e,i,*], R. Sadat [f], C.B. Odetunde [g], O.A. Ajala [h], A.O. Akindele [h]

[a] Department of Mathematical Sciences, Augustine University Ilara-Epe, Lagos, Nigeria
[b] Department of Mathematics, BOWEN University, Nigeria
[c] Department of Mathematics and Social Sciences, Sukkur IBA University, Sukkur, 65200, Sindh, Pakistan
[d] School of Engineering, Cranfield University, Cranfield, UK
[e] Faculty of Engineering and Technology, Future University in Egypt, New Cairo, 11835, Egypt
[f] Department of Mathematics, Zagazig Faculty of Engineering, Zagazig University, Egypt
[g] Faculty of Engineering, Augustine University Ilara-Epe, Lagos, Nigeria
[h] Department of Pure and Applied Mathematics, Ladoke Akintola University of Technology, Nigeria
[i] Basic Engineering Science Department, Benha Faculty of Engineering, Benha University, Benha, Egypt

ARTICLE INFO

Keywords:
Hybrid nanofluid
Entropy generation
Galerkin weighted residual method (GWRM)
Parabolic trough solar collector (PTSC)
Surface combatants

ABSTRACT

This study examines the potential of using nanofluids in solar thermal energy systems. Nanofluids are known to exhibit high convection heat transfer coefficients, low specific heat, and density, making them ideal for improving the performance of solar thermal energy systems. However, this computational study investigates the application of Cattaneo-Christov heat flux on cylindrical surfaces using carbon nanotube (CNT) hybrid nanofluids, for use in a solar-powered ship. The work utilizes numerical simulations to analyze the heat transfer and fluid flow characteristics of the hybrid nanofluids. The research examines the use of single-walled and multi-walled carbon nanotubes (SWCNT and MWCNT) in engine oil (EO) as the working fluid. The Galerkin weighted residual method (GWRM) is utilized to solve the ordinary differential equations (ODEs) governing the system. The impact of various parameters, such as Cattaneo-Christov heat flux, solar thermal radiation, nonlinear stretching surface, slippery velocity, and porous media on the velocity equation, energy equation, and entropy generation are investigated and elaborated through detailed plots. The findings show that the MWCNT-SWCNT/EO hybrid nanofluid (HNF) exhibits maximum efficiency of around 2.4%, while the minimum efficiency is at 2.7%. This research provides valuable insights into the design and optimization of solar thermal systems for sustainable transportation.

* Corresponding author. Faculty of Engineering and Technology, Future University in Egypt, New Cairo, 11835, Egypt.
E-mail addresses: adebowale.obalalu17@gmail.com (A.M. Obalalu), kunlesalawu2@gmail.com (S.O. Salawu), asif-memon@iba-suk.edu.pk (M.A. Memon), Olalekan.a.Olayemi@cranfield.ac.uk (O.A. Olayemi), mohamed.reda@fue.edu.eg (M.R. Ali), r.mosa@zu.edu.eg (R. Sadat), Debospecial@gmail.com (C.B. Odetunde), oaajala@lautech.edu.ng (O.A. Ajala), aoakindele65@pgschool.lautech.edu.ng (A.O. Akindele).

https://doi.org/10.1016/j.csite.2023.102959
Received 7 February 2023; Received in revised form 25 March 2023; Accepted 27 March 2023
Available online 7 April 2023

1. Introduction

In recent years, renewable energy have received significant attention because of the depletion of fossil fuels and the increase in the cost of conventional forms of energy, such as electricity [1]. The combustion of fossil fuels releases carbon dioxide into the atmosphere, whereas the generation of electricity from renewable sources does not contribute to the emission of greenhouse gases [2].In addition, according to environmentalists, the utilization of renewable energy sources can assist in reducing carbon emissions and global warming [3]. In the last few decades, solar energy has gotten a lot of attention as a possible alternative source of renewable energy since it is available, pollutant-free, and has the least negative effects on the environment [4,5]. Sun-based energy is the most sustainable, accessible, and environmentally friendly form of energy that can be harnessed here on earth. Sun-based energy has the potential to generate 4xmegawatts of power, which is about two hundred times (200) greater than the quantity of electricity that is currently consumed on a worldwide scale [3]. In comparison to 1985 levels, new research predicts that global CO_2 emissions will be reduced by 75% by the year 2050 [6]. According to research conducted by the United States Department of Energy, the annual energy needs of the entire planet could be met by the direct sunlight reaching the earth's surface for only one and a half hours [6]. This finding was published in a US report. However, solar energy will serve as a natural alternative energy source. solar systems also provide thermal energy for use in domestic appliances [7]. Therefore, the main question is how to absorb energy from the sun.

Photovoltaic (PV) systems and Concentrated solar energy (CSE) are the two primary methods for converting sunlight into electricity [8]. The following are some of the most essential applications that can be achieved using PV systems: (a) Solar power plants [9] (b) satellite power generators in spacecraft [10], and (c) Remote area power supply (RAPS),which includes generators, streetlights, and radio transmitters [11]. The principal component of a photovoltaic device's is an example of a semiconductor, which is a type of material that can carry numerous electrons. The capacity of the solar cell surface to absorb light from the sun causes electrons to vibrate, leading to the creation of electrical current as they move through the semiconductor device. Concentrated solar power is a technology that uses concentrated sun-based energy and is usually used in agriculture (concentrating solar power plant). The following is the process in which energy is transformed by concentrated solar power: massive mirrors are used to focus the light of the sun or lenses, after which it performs a transformation to become heat (thermal energy), and lastly, electricity is produced once the heat has gone through an electrical power generator. Desert locations, such as California and Arizona in the United States, are suitable for developing larger plants with concentrated solar power because of the climate [12]. It is better than other forms of energy since it is renewable and does not contribute to the discharge of hazardous pollutants. In summary, sun-based energy is chosen over other forms of energy since it is a renewable resource that does not produce harmful pollution, unlike fossil fuels.

Meanwhile, about three percent of the world's total carbon dioxide emissions are caused by commercial shipping operations that use heavy fuel oil (HFO) and marine diesel oil (MDO) [13]. Approximately 932 million tons of these pollutants were released into the atmosphere in 2015. As a point of reference, the total emissions produced by Germany in 2017 amounted to 905 million tons [14]. The exhaust emissions from these ships contain many pollutants that are hazardous to human physical condition, the environment, and the weather [15]. In addition, the exhaust emissions from heavy fuel oil combustion contain Sulphur oxide, which contains combustion products, nitrogen oxides, and heavy metals (CO2) [16]. These substances are responsible for a portion of the pollution that occurs in the ocean. The major causes of pollution from ships are illustrated in Fig. 1a [17]. Recently, scientists have started investigating the use of solar power to minimize the amount of greenhouse gas emissions from merchant ships. However, the use of sun-based energy in marine power systems is commonly considered an attractive solution for many countries since it paves the way for the creation of green ships. The incorporation of PV energy into a marine power plant requires an in-depth knowledge of the electrical power system and several other components of shipping. The MS Tûranor Planet Solar is the world's biggest sun-based ship, which was unveiled on March 31, 2010. It was created by Raphael Domjan. It began its journey in May 2010 and completed it in May 2012, making it the first solar-powered electric ship to ever complete a full round of the world [18]. The solar powered ship set sail from the western direction of Monaco on September 27, 2010, intending to complete its journey around the world using only the electricity provided by the sun. It travels continuously for up to 72 h, and the ship's engines are powered by sun-based energy. One of the goals of the initiative was to increase people's knowledge of the significance of using renewable energy sources to safeguard the environment. These kinds of events draw more attention to the scientists investigating the solar-powered ship. The report by Kirkpatrick [19] studied the performance of

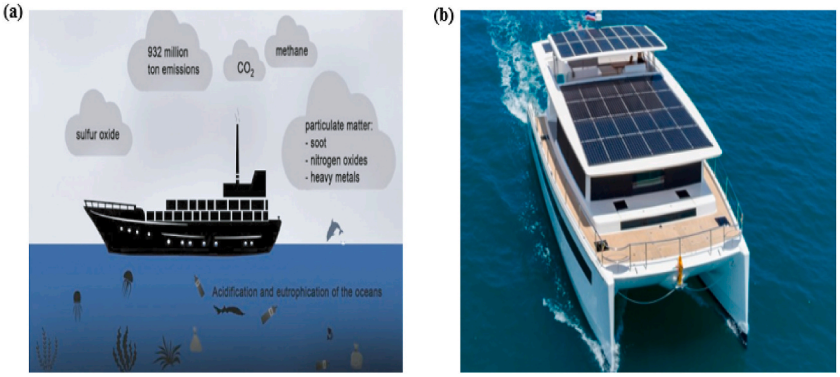

Fig. 1. (a) Display the ship emissions with some consideration for the ocean,(b) Sun-based ship.

photovoltaic systems on surface combatant ships that were installed on Navy ships. Their research showed that the extra weight added by solar cellis quite minimal compared to the amount of supplies fuel, and food that a ship has to carry when it sets sail. The work of Cristea [20] shows the findings of testing the efficiency of photovoltaic cell modules aboard a ship, both when the ship was moving and while it was stationary. Their research showed that without an azimuth sun tracking device, a solution that is 30° off the horizontal cannot be put into place. Therefore, a better option would be a zero-degree angle. The sun-based generation aboard less extensive fishing boats operating in remote waters was investigated by Ref. [21]. The results indicate that the additional drag caused by the aerodynamics of the panels mounted on the wheelhouse is another characteristic that may influence fuel usage, particularly given that the boat operates in windy weather. Yufang et al. [22] researched the concept of a fuel-free spacecraft that operates on energy provided by the sun and the wind. The relationship between a theoretical and practical photovoltaic system on a testing ship was investigated by Cristea et al. [23]. They observed that horizontally oriented solar panels had a greater overall efficiency rating than vertically oriented panels. The research conducted by Hussein et al. [24] demonstrates that there is a potential for using photovoltaic systems as a method on the ship to provide renewable energy in order to eliminate the need for fossil fuels. Lan et al. [25] proposed a method for determining the optimal proportion of the photovoltaic system mixing methodology for ship power operations in order to help reduce financing, fuel costs, and engine pollution. Also, the authors did more research on improving the slope-angle featured in the photovoltaic panels located on a huge oil transporter ship. Fig. 1b depicts a sun-powered energy ship [26].

Nanofluid (NF) is among the most widely utilized working fluids in parabolic trough solar collectors [27]. It is described as a mixture of nanoparticles (NPs) (whether metal or non-metal) and base-fluid (BF) (hydrogen and oxygen, oil, ethylene glycol) [28]. Metallic NPs include copper, iron, zinc, aluminum, and gold, while non-metallic NPS include single-wall carbon nanotubes (SWCNT), silicon dioxide, titanium dioxide, iron oxide, multi-wall carbon nanotubes (MWCNT) ferric oxide, zinc oxide, cerium dioxide, carbon nanotubes (CNT) [29]. The utilization of NF has the potential to advance the thermal effectiveness achieved by the operational structure in parabolic trough solar collectors [30]. However, the following are some of the significant factors that contribute to making NF an effective working fluid: (a) the kind of based fluid and nanoparticles; (b) the shape, size, and volume proportion of the NPs; and (c) the NF's radiative properties, and consistency [31,32]. Consequently, the use of NF as a working fluid in PTSC has been reported experimentally [33,34] and computationally. The nanofluid experimental investigation shows that parabolic trough solar collectors' performance can be improved by using materials like Aluminum oxide/water NF, Multi-walled carbon nanotubes/mineral, Copper (II) oxide/H20, Copper (II) oxide/Ethylene glycol, Titanium dioxide/H20, MWCNT/Ethylene glycol, and Silicon dioxide/Ethylene glycol. In summary, Multi-walled carbon nanotubes (non-metallic NF) and Copper (metallic NF) are the NPs that contribute most to thermal performance [35]. The cobalt (II, III) oxide NPs on the NF chosen by Ref. [36] were synthesized via the endophytic fungus Aspergillus nodulins in their experimental study. They investigated the absorption rate and photothermal conversion capability differences between nanofluid and water. However, the preferable choice of cobalt (II, III) oxide NPs over pure water showed that NPs are the preferable choice for solar power systems. Sundar et al. [37] investigated the effects of nanofluids and wire coils (Aluminum Oxide NF and wire coil with core rod inclusions) on a solar flat plate absorber. Ganesh et al. [35] created a solar glycol (SG)–H2 NF containing alumina NPs to analyze NF that features electrical conductivity, stability, density, viscosity, and thermal conductivity. Their research revealed that NF has a greater amount for storing energy and transporting heat. Effect of Cattaneo-Christov heat flux on heat and mass transfer characteristics of Maxwell hybrid nanofluid flow over stretching/shrinking sheet was study by Ref. [38]. Soret and Dufour effects on unsteady MHD heat and mass transfer from a permeable stretching sheet with thermophoresis and non-uniform heat generation/absorption was investigated by Ref. [39]. Entropy generation and heat transfer analysis of magnetic hybrid nanofluid inside a square cavity with thermal radiation was examined by Ref. [40]. Maxwell hybrid nanoliquid flow over vertical cone with Cattaneo-Christov heat flux and convective boundary condition was investigated by Ref. [41].

In addition to the NPs described above, CNTs (carbon nanotubes) are also considered to be NPs. Carbon is the element that is used to make CNT. Carbon nanotubes are regarded as one of the strongest light-absorbing materials because of their distinctive electrical, optical, and mechanical characteristics [3,4]. In addition, carbon nanotubes have a great level of both physical and chemical stability, as well as a large area of surface and a greater amount of thermal conductivity [5]. There are two different kinds of CNTs, categorized as MWCNT (multi-walled carbon nanotube) and SWCNT (single-walled carbon nanotube). The MWCNT has a collection of nested tubes with a continually increasing diameter, whereas the SWCNT only has a single wall or layer. However, the impact of carbon nanotube coating on the performance of parabolic trough solar collectors has been investigated. The MWCNT/water NF was used by Hachicha et al. [42] to simulate the performance of parabolic trough solar collectors under various seasonal conditions. According to the outcomes of their simulations, the utilization of NF leads to a maximum improvement of 21% points in the Nusselt number. The engineering equation solver software was used by Bellos et al. [43] to conduct an investigation of NF-based PTSCs with the intent of enhancing thermal efficiency. Their simulation results showed that the highest thermal improvement was achieved between 4% and 17%. Combined influence of Brownian motion and thermophoresis on Maxwell three-dimensional nanofluid flow over stretching sheet with chemical reaction and thermal radiation was investigated by Ref. [44]. Williamson hybrid nanofluid flow over swirling cylinder with Cattaneo–Christov heat flux and gyrotactic microorganism was investigated by Ref. [45]. Impact of homogeneous–heterogeneous reactions on heat and mass transfer flow of Au–Eg and Ag–Eg Maxwell nanofluid past a horizontal stretched cylinder was study by Ref. [46]. A narrative loom of hybrid nanofluid-filled wavy walled tilted porous enclosure imposing a partially active magnetic field was study by Ref. [47]. Magneto-hydrothermal convective dynamics of hybrid nanofluid packed partially cooled porous cavity was study by Ref. [48]. Enhanced energy and mass transport dynamics in a thermo-magneto-bioconvective porous system containing oxytactic bacteria and nanoparticles was study by Ref. [49]. Magneto-hydrothermal triple-convection in a W-shaped porous cavity containing oxytactic bacteria was investigated by Ref. [50].

Hybrid NPs consist of two or more distinct nanometer-sized materials as NPs. Fluids can be generated by utilizing hybrid nanomaterials, and these fluids are described as hybrid nanofluids (HNF) [4,5]. The major advantage of adopting a hybrid nanofluid in a

solar energy system is that an increase in thermal conductivity leads to an increase in heat transfer rate. The main benefit of using a hybrid nanofluid in a solar-powered system is an increment in the efficacy of the solar system, which can be as high as sixty percent in certain circumstances [51]Since an increase in thermal conductivity produces a greater heat transfer rate. Also, adding hybrid nanofluids in the form of an occupied fluid to a solar energy system would improve the system's optical characteristics, which would make the system work better [55]. Investigations of HNF in solar concentrators and collectors have been previously carried out by the following scientific research: the study on Copper(II) oxide/Aluminium oxide hybrid nanofluids with an ethylene glycol-based fluid, Silicon dioxide-Copper(II) oxide/Ethylene glycol HNF, Titanium dioxide-silver/water HNF, the HNF Aluminium oxide and Titanium dioxide with the BF Therminol-55 oil. To conclude, these kinds of hybrid nanoparticles and their concentration have a major influence on the performance of the solar energy generation system, and the suitable hybrid nanofluid must be selected with consideration given to both their thermal and optical characteristics. Gupta et al. [52]researched the flow of Zinc ferrite/water NF inside of a circular tube. The investigation of heat transmission was discussed via [63], and its findings included thermal characteristics, validation, heat transfer coefficient of Nusselt number, and pressure loss property. Meanwhile, the lack of research pertaining to the use of hybrid nanofluids in parabolic trough solar collectors [53] is due to the perception that this area is new and most recent. The work of Mineaet al. [54] used numerical study to show that the silver- Magnesium oxide /water HNF is the most effective working fluid in parabolic trough solar collectors when compared to the other two HNF (graphene oxide-cobalt (II, III) oxide/60 EG:40W and copper-aluminum oxide/water). Recent contributions addressing NF with heat and mass transport in different physical conditions are reported by Refs. [55–58]. Hybrid nanofluid magnetohydrodynamic mixed convection in a novel W-shaped porous system [59].

Magneto-hydrothermal performance of hybrid nanofluid flow through a non-Darcian porous complex wavy enclosure [60]. Role of surface undulation during mixed bioconvective nanofluid flow in porous media in presence of oxytactic bacteria and magnetic fields [61]. Thermo-fluidic transport process in a novel M-shaped cavity packed with non-Darcian porous medium and hybrid nanofluid: Application of artificial neural network (ANN) [62].

According to the principle of viscosity, there are two types of fluids: Newtonian and non-Newtonian fluids (NNF). NNF flows have captured the attention of researchers in recent years due to their practical uses. The wide range of NNF is used in many fields, such as the biological sciences, technology, chemical, and petroleum industries. However, the Navier–Stokes formulas are not capable of providing an accurate description of the NNF flow. The constitutive equations can provide accurate predictions about the rheological properties. It is essential to investigate the fluid properties of non-Newtonian fluids to get an accurate knowledge of these fluids. Because of the complexity of the problem, there is not a single constitutive equation that can accurately model all of the features of non-Newtonian fluids. However, most NNF models in academic papers focus on simple models such as rheological power laws and second and third-grade fluid, Casson fluid [63–66]. When it pertains to modeling liquids with shear-dependent viscosity, the power-law model is one of the most used choices among researchers. Therefore, it is incapable of predicting the influence of that elasticity. Furthermore, the fluids of grades two or three can provide the impact of elasticity when applied properly. However, shear dependence does not influence the viscosity of these models. Also, second and third-grade fluid is incapable of predicting the influences of stress relaxation. The non-Newtonian fluids Maxwell model, which belongs to the category of rate-type fluids, can forecast stress relaxation. As a result, these fluids have gained more and more popularity [67–69]. The computational study of viscoelastic coolant Maxwell fluid and CNTs hybrid nanoparticle on a PTCS [70]. The thermal characterization of two-dimensional Maxwell nanofluid flow over a permeable stretching sheet using the finite element method [71,72].

Sun-based energy has become an increasingly significant source of electricity in developing countries due to its relative availability compared to other kinds of energy. Sun-powered ships and boats offer the benefits of being ecologically friendly, inexpensive, reducing

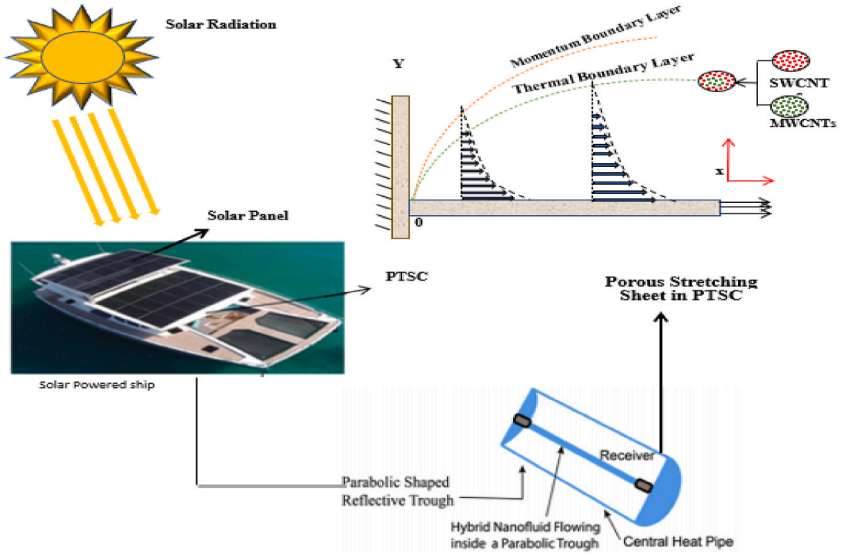

Fig. 2. The current theoretical test for the sun-based ship.

noise exposure, capable of charging continuously, assisting in the restoration of a ship's dead battery, minimizing negative effects on the environment, and most importantly, they are dependable. Numerous studies have highlighted the need for detailed entropy and thermal analysis of solar power systems. Furthermore, the use of nanofluids in PTSCs is crucial to improving the system's performance. In this research, the Cattaneo–Christov model was utilized to investigate the behavior of a viscous Maxwell nanofluid as it moved across an infinite heat flux-produced horizontal surface. A mixture of NNF nanofluids, SWCNT-EO, and MWCNT-EO is used to increase the thermal efficiency of PTSC. Furthermore, this research investigates the effect of dimensionless numbers on entropy production. This preliminary theoretical experiment has not yet been carried out in any way. By using the light and heat from the sun, the PTSC can serve as a significant source of energy for the navy surface combatant's ship. Fig. 2 presents a diagrammatic representation of the PTSC using hybrid nanofluid.

2. Model equations

The investigation of the Maxwell HNF flow describes the moving horizontal flat solid surface with non-uniform extending velocity [26]:

$$\mathrm{U_w}(\mathrm{x},0) = bx \tag{1}$$

In this case, b is a preliminary extending ratio. Then, the insulated surface temperature indicated as T_w (x, t) $= \mathrm{T}_\infty + b^* x$, and assumed to be fixed at $x = 0$. In addition, $b^* x$ indicate as thermal charge rate, T_w is wall temperature, T_∞ stand for the ambient temperature.The HNF is synthesized by the adding SWCNT Nano-sized particles in engine oil-BF for fractional volume φ_{SWCNT} and it is made secure at 0.09 all over in the present study. It is assumed that the surface is both slippery and experiencing a temperature difference. Fig. 3geometrical diagram of the flow.

The mathematical model of the Maxwell HNF model along with properties of porous media, Cattaneo-Christov heat flux, and thermal radiation are:

$$\frac{\partial \nu_1}{\partial x} + \frac{\partial \upsilon_2}{\partial y} = 0 \tag{2}$$

$$\upsilon_1 \frac{\partial \nu_1}{\partial x} + \upsilon_2 \frac{\partial \nu_1}{\partial y} = \frac{\mu_{hnf}}{\rho_{hnf}} \left[\frac{\partial^2 \upsilon_1}{\partial y^2}\right] - \frac{\mu_{hnf}}{\rho_{hnf^k}} \upsilon_1 - \varsigma \left[{\upsilon_1}^2 \frac{\partial^2 \upsilon_1}{\partial x^2} + {\upsilon_2}^2 \frac{\partial^2 \upsilon_1}{\partial y^2} + 2\upsilon_1 \upsilon_2 \frac{\partial^2 \upsilon_1}{\partial x \partial y} \right] \tag{3}$$

$$\begin{aligned} \upsilon_1 \frac{\partial T}{\partial x} + \upsilon_2 \frac{\partial T}{\partial y} = {} & \frac{1}{(\rho C_p)_{hnf}} \left[k_{hnf} \left(\frac{\partial^2 T}{\partial y^2} \right) - \left(\frac{\partial q_r}{\partial y} \right) + \mu_{hnf} \left(\frac{\partial \nu_1}{\partial x} \right)^2 + Q(T - \mathrm{T}_w) \right] \\ & + \xi \left[\upsilon_1 \left(\frac{\partial \nu_1}{\partial x} \frac{\partial T}{\partial x} \right) + \upsilon_2 \left(\frac{\partial \nu_2}{\partial y} \frac{\partial T}{\partial y} \right) + \upsilon_1 \left(\frac{\partial \nu_2}{\partial x} \frac{\partial T}{\partial y} \right) + \upsilon_2 \left(\frac{\partial \nu_1}{\partial y} \frac{\partial T}{\partial x} \right) + \upsilon_1^2 \left(\frac{\partial^2 T}{\partial x^2} \right) + \upsilon_2^2 \left(\frac{\partial^2 T}{\partial y^2} \right) + 2\upsilon_1 \upsilon_2 \frac{\partial^2 T}{\partial x \partial y} \right] \end{aligned} \tag{4}$$

Subjected to:

$$\begin{aligned} \upsilon_1(\mathrm{x},0) &= U_w + P_w \left(\frac{\partial \nu_1}{\partial y} \right) \\ \upsilon_2(\mathrm{x},0) &= R_\mathrm{w} \\ -k_0 \left(\frac{\partial T}{\partial y} \right) &= h_g (T_w - T) \upsilon_1 \longrightarrow 0, T \longrightarrow T_\infty, \text{as} \quad y \longrightarrow \infty. \end{aligned} \tag{5}$$

In the above equations, the flow velocity indicates the components are $\overleftarrow{\upsilon} = [\upsilon_1(x,y), \upsilon_2(x,y), 0]$. $T, \xi, Q, P_w, R_\mathrm{w}, k_g, h_g,$ *and* ς indicates the fluid heat,thermal relaxation, heat generation, slip length, surface permeability, the porousness of material, the heat transport factor, and fluid relaxation respectively.

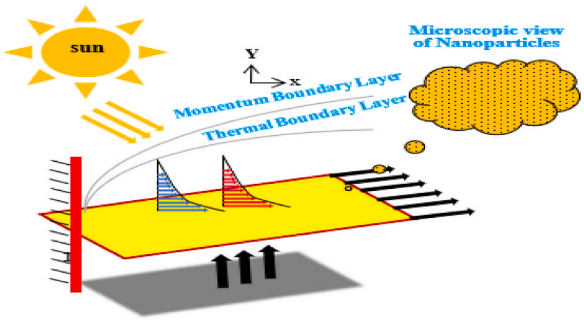

Fig. 3. Geometrical diagram of the flow.

2.1. Thermophysical properties of nanofluid and hybrid nanofluid [73]

$$\mu_{nf} = \frac{\mu_f}{(1-\varphi)^{2.5}}$$

$$\rho_{nf} = (1-\varphi)\rho_f - \varphi\rho_s$$

$$(\rho C_p)_{nf} = (1-\varphi)(\rho C_p)_f - \varphi\,(\rho C_p)_s$$

$$\frac{k_{hnf}}{k_{gf}} = \frac{(k_s + 2k_f) - 2\varphi(k_f - k_s)}{(k_s + 2k_f) + \varphi(k_f - k_s)} \tag{6a}$$

Hybrid nanofluid:

$$\mu_{hnf} = \mu_f / (1 - (\varphi_1 + \varphi_2))^{2.5} \tag{6b}$$

$$\rho_{hnf} = (1 - (\varphi_1 + \varphi_2))\rho_f + \varphi_1\rho_{s_1} + \varphi_2\rho_{s_2}$$

$$(\rho C_p)_{hnf} = (1 - (\varphi_1 + \varphi_2))(\rho C_p)_f + \varphi_1(\rho C_p)_{s1} + \varphi_2(\rho C_p)_{s2}$$

$$\frac{k_{hnf}}{k_{nf}} = \left(\frac{(k_{s2} + 2k_{nf} - 2\varphi_2(k_{nf} - k_{s2})}{(k_{s2} + 2k_{nf} + \varphi_2(k_{nf} - k_{s2})}\right),$$

$$\frac{k_{nf}}{k_f} = \left(\frac{k_{s1} + 2k_f - 2\varphi_1(k_f - k_{s1})}{(k_{s1} + 2k_f + \varphi_1(k_f - k_{s1})}\right).$$

In equations (6) and (7), μ_{hnf}, ρ_{hnf}, $(\rho C_p)_{hnf}$, k_{hnf} indicates the viscosity, density, Specific heat, and thermal conductivity respectively. $\varphi_{nf}\varphi_{hnf}$ is the solid-particle concentration of MWCNT and SWCNT.

2.2. Nanoparticles (NPs) and base fluid (BF) features

The physical features of BF Engine oil (EO), Single-walled carbon nanotubes (SWCNT), and Multiwalled carbon nanotube (MWCNT) NPs are revealed in Table 1.

Several engineering applications include biochemical sensitivity, coal-based manufacturing structures, direct solar collectors, power generation, plate, shell, and tube type heat exchangers for ships, heating, ventilation, air conditioning automobile radiators, and aircraft radiators. Therefore, these applications require heat transport of fluids. Heat exchangers are essential to the operation of any system, so they must function properly. However, there are a lot of techniques that have been utilized to increase their efficiency. The performance of these technologies is often limited by how well heat moves through the system. For instance, engine oil (EO) is a liquid hydrocarbon, fuel combustion, semi-synthetic oil, and engine oil mixability, whichhas received a lot of attention. Engine oil has important advantages; many components of an engine need to be lubricated with engine oil to minimize friction and loss of energy. Also, it helps prevent corrosion and rust, making the engine smoother, producing a layer that protects the metal components from wear, and enhancing the flow properties of the oil.

2.3. Calculation of Rosseland Approximation (RA)

To incorporate the radiative influence, equation (4) makes use of the RAform [67], and it is written as follows:

$$qr = -\frac{4\sigma^*}{3k^*}\frac{\partial\omega}{\partial y} \tag{7}$$

σ^* described as Stefan Boltzmannand k^* signifies the absorption coefficient.

2.4. Similarity transformation

The transformation quantities and stream functions are defined as:

Table 1
The physical characteristics of the base fluid and hybrid nanofluid [74]

Physical property	Engine oil (EO)	MWCNT	SWCNT
$\rho/\ (kg.m^{-3})$	884	1600	2600
$k/\ (W.mK)$	0.14	3000	6000
$C_p/\ (J.kgK)$	1910	796	425

$$\theta(\gamma)=\frac{T-T_{\infty}}{T_w-T_{\infty}}, \gamma(x,y)=\sqrt{\frac{b}{\upsilon_f}}y\ \psi(x,y)=\sqrt{\upsilon_f b}xf(\gamma), \tag{8}$$

and

$$\upsilon_1=\frac{\partial\psi}{\partial y}; \text{and } \upsilon_2=-\frac{\partial\psi}{\partial x} \tag{9}$$

2.5. Transformed problems

The momentum and thermal characteristics of an SWCNT (multi-walled carbon nanotube/water)-based hybrid nanofluid are plugged by the transformation.

$$\Lambda_N f'''f^2+\frac{1}{\varphi_a\varphi_b}K_N f'-f'f''-\frac{f'''}{\varphi_a\varphi_b}-\Lambda_N(2ff'f'')+f'^2=0 \tag{10}$$

$$\theta''\left(1+\frac{1}{\varphi_d}Pr\ R_N\right)+\Pr\frac{\varphi_c}{\varphi_d}\left[f\theta'-f'\theta+\frac{\mathrm{Ec}}{\varphi_a\varphi_c}f''^2+\theta\frac{Q_N}{\varphi_c}-\delta_N f'^2\theta+\delta_N\left(\theta f''+\theta^2f^2+ff''\theta''\right)\right]=0 \tag{11}$$

Subjected to

$$f(0)=S, f'(0)=1+\varpi_N f''(0), f'(\gamma)\longrightarrow 0, \theta'(0)=-B_i(1-\theta(0)), \theta(\gamma)\longrightarrow 0 \quad , \text{as} \quad \gamma\longrightarrow\infty, \tag{12}$$

Where

$$\varphi_a=(1-(\varphi_1+\varphi_2))^{2.5},$$

$$\varphi_b=(1-(\varphi_1+\varphi_2))+\varphi_1\rho_{s_1}/\rho_f+\varphi_2\rho_{s_2}/\rho_f$$

$$\varphi_c=(1-(\varphi_1+\varphi_2))+\varphi_1(\rho C_p)_{s1}/(\rho C_p)_f+\varphi_2(\rho C_p)_{s2}/(\rho C_p)_f,$$

$$\varphi_d=\left(\frac{(k_{s2}+2k_{nf}-2\varphi_2(k_{nf}-k_{s2})}{(k_{s2}+2k_{nf}+\varphi_2(k_{nf}-k_{s2})}\right)\times\left(\frac{k_{s1}+2k_f-2\varphi_1(k_f-k_{s1})}{(k_{s1}+2k_f+\varphi_1(k_f-k_{s1})}\right).$$

2.6. Explanation of the entrenched control constraints

The thermophysical features of Maxwell HNF and the symbols utilized in the current investigation are detailed in Table 2.

Table 2
below lists the governing equation's control parameters.

Parameters	Formula	Symbols
Biot number	$B_i=\frac{h_f}{k_o}\sqrt{\frac{\upsilon_f}{b}}$	B_i
Eckert number	$E_N=\frac{U_w^2}{(C_p)_f(T_w-T_\infty)}$	E_N
Heat generation	$Q_N=\frac{Q_0}{(\rho C_p)_f b}$	Q_N
Solar radiation parameter	$R_N=\frac{16}{3}\frac{\sigma^* T_\infty^3}{k^*\upsilon_f(\rho C_p)_f}$	R_N
Suction/Injection Parameter	$S=-R_w\sqrt{\frac{1}{\upsilon_f b}}$	S
velocity slip	$\varpi_N=\sqrt{\frac{b}{\mu_f}}P_w$	ϖ_N
Prandtl number	$\Pr=\frac{\upsilon_f}{\alpha_f}$	Pr
Porous medium	$K_N=\frac{\upsilon_f}{bk}$	K_N
Non-Newtonian Maxwell	$\Lambda_N=\mathrm{b}\,\varsigma$	Λ_N
Relaxation time	$\delta_N=\mathrm{b}\,\xi$	δ_N
thermal diffusivity	$\alpha_f=\frac{k_f}{(\rho C_p)_{hnf}}$	α_f
Entropy generation	$N_G=\frac{E_G\mathrm{b}^2T_\infty^2}{k_f(\mathrm{T}_w-\mathrm{T}_\infty)^2}$	N_G

2.7. Physical quantities

The drag-force (C_f) and Nusselt number (Nu_x) are the physical quantities requirements for the practicality and utility of engineering, and can be defined as follows:

$$C_f = \frac{\tau_w}{\rho_{hnf} U_w^2}, \text{ and } Nu_x = \frac{x q_w}{k_f(\mathrm{T}_w - \mathrm{T}_\infty)}, \tag{13}$$

The results of the application of non-dimensional transformations (8) are represented as follows:

$$\begin{gathered} Re_x^{1/2} C_f = \frac{1}{\varphi_a} f''(0) \\ \text{And} \\ Re_x^{1/2}\, Nu_x = -\frac{k_{hnf}}{k_f}[(1+R_N)\theta'(0)] \end{gathered} \tag{14}$$

where local Reynolds number *is* $Re_x = \frac{U_w x}{\nu_f}$.

3. Entropy generation analysis

The entropy production in HNF is defined as:

$$N_G = Re\left[\varphi_d(1-Nr)\theta'^2 + \frac{1}{\varphi_a}\frac{B_N}{\beta}\left(f''^2 + Kf'^2\right)\right], \tag{15}$$

In the above equation the, $\beta = \frac{\mathrm{T}_w - \mathrm{T}_\infty}{\mathrm{T}_\infty}$ is the difference in temperatures, $B_N = \frac{\mu_f u_w^2}{k_f(\mathrm{T}_w - \mathrm{T}_\infty)}$ is Brinkmann number, $\mathrm{Re} = \frac{u_w b^2}{x\upsilon_f}$ is Reynolds number.

4. Numerical Solution

4.1. Galerkin Weighted Residual Method (GWRM): a summary

Several linear and nonlinear physical issues in physics and engineering, such as the fluid flow of heat transfer in an infinite domain, are subjecte to boundary conditions at infinity. This is the case regardless of the kind of problem.To find solutions to problems that occurred in semi-infinite domains, the approach of weighted residual is applied. Where subdomains were generated by dividing the domains, the Simpson rule was used to integrate the parts of the subdomains that were finite, and the shifted Laguerre method was used to integrate the infinite parts.

4.2. Application of (GWRM)

The numerical solutions to equations 10–12 are obtained using the GWRM. The concepts of solving various GWRM are discussed in Ref. [5]. The key step of the GWRM are listed below:

Stepone, examine the equations (10)-(11)

$$\Lambda_N f''' f^2 + \frac{1}{\varphi_a\varphi_b} K_N f' - f' f'' - \frac{f'''}{\varphi_a\varphi_b} - \Lambda_N(2ff' f'') + f'^2 = 0 \tag{16}$$

$$\theta''\left(1 + \frac{1}{\varphi_d} Pr\, R_N\right) + \mathrm{Pr}\frac{\varphi_c}{\varphi_d}\left[f\theta' - f'\theta + \frac{\mathrm{Ec}}{\varphi_a\varphi_c} f''^2 + \theta\frac{Q_N}{\varphi_c} - \delta_N f'^2\theta + \delta_N\left(\theta f'' + \theta^2 f^2 + ff''\theta''\right)\right] = 0 \tag{17}$$

In step two,The trail function are used to simulate the numerical result of equations(15) and (15) which include a linear combination of basic functions as shown below:

$$\widetilde{f}(\gamma) = q_0 + q_1 e^{-\frac{\gamma}{3}} + q_2 e^{-\frac{2\gamma}{3}} + \ldots\ldots\ldots + q_n e^{-\frac{n\gamma}{3}} = \sum_{i=0}^{n} q_i e^{-\frac{i\gamma}{3}}, \tag{18}$$

$$\widetilde{\theta}(\gamma) = s_0 + s_1 e^{-\frac{\gamma}{3}} + s_2 e^{-\frac{2\gamma}{3}} + \ldots\ldots\ldots + s_n e^{-\frac{n\gamma}{3}} = \sum_{i=0}^{n} s_i e^{-\frac{i\gamma}{3}}, \tag{19}$$

Step two, the proposed trial solutions through the GWRM must satisfy the corresponding BCs for equation (10)-(11).By using the BCs in equation (12).we were able to come up with the following trial solutions:

$$\left(\sum_{i=0}^{n} q_i e^{-\frac{i\gamma}{3}} - S\right)_{\gamma=0} = 0$$

$$\left(\frac{d}{d\gamma}\sum_{i=0}^{n} p_i e^{-\frac{i\gamma}{3}} - \varpi_N \frac{d^2}{d\gamma^2}\sum_{i=0}^{n} p_i e^{-\frac{i\gamma}{3}} - 1\right)_{\gamma=0} = 0 \tag{20}$$

$$\left(\frac{d}{d\gamma}\sum_{i=0}^{n} s_i e^{-\frac{i\gamma}{3}} + B_i\left(1 - \frac{d}{d\gamma}\sum_{i=0}^{n} s_i e^{-\frac{i\gamma}{3}}\right)\right)_{\gamma=0} = 0$$

In step four, In the Galerkin technique, the residual vectors for fluid-fluid $f(\gamma)$ and heat flow $\theta(\gamma)$ are constructed as shown below by inserting the trial solutions (20) into the equation that was presented in step One.

$$R_f = \Lambda_N \widetilde{f}''' \widetilde{f}^2 + \frac{1}{\varphi_a \varphi_b} K_N \widetilde{f}' - \widetilde{f}' \widetilde{f}'' - \frac{f'''}{\varphi_a \varphi_b} - \Lambda_N (2\widetilde{f}\widetilde{f}'\widetilde{f}'') + \widetilde{f}'^2 \cong 0 \tag{21}$$

$$\widetilde{\theta}''\left(1 + \frac{1}{\varphi_d} Pr\, R_N\right) + \Pr \frac{\varphi_c}{\varphi_d}\left[\widetilde{f}\widetilde{\theta}' - \widetilde{f}'\widetilde{\theta} + \frac{\mathrm{Ec}}{\varphi_a \varphi_c}\widetilde{f}''^2 + \widetilde{\theta}\frac{Q_N}{\varphi_c} - \delta_N \widetilde{f}'^2 \widetilde{\theta} + \delta_N\left(\theta f'' + \theta^2 f^2 + \widetilde{\theta}\widetilde{f}'' + \widetilde{\theta}^2 \widetilde{f}^2 + \widetilde{f}\widetilde{f}''\widetilde{\theta}''\right)\right] = 0 \tag{22}$$

Step five,the residual must be equal to zero:

$$\int_0^{\infty} R_f e^{-\frac{i\gamma}{3}} d\eta \approx \sum_{k=1}^{i}\left[A_k\left(e^{\gamma} R_f e^{-\frac{i\gamma}{3}}\right)_{\gamma=x_k}\right] = 0, \int_0^{\infty} R_\theta e^{-\frac{i\gamma}{3}} d\eta \approx \sum_{k=1}^{i}\left[s_k\left(e^{\gamma} R_\theta e^{-\frac{i\gamma}{3}}\right)_{\eta=x_k}\right], = 0, \tag{23}$$

For $i = 0, 1, 2, \ldots, N-2, l = 0, 1, 2, \ldots, N-2$ to zero

$$A_k = \frac{1}{L_j'(x_k)}\int_0^{\infty} \frac{L_j(x)e^{-x}}{x - x_k} dx = \frac{(j!)^2}{x_k\left(L_j'(x_k)\right)^2}, L_j = e^x \frac{d^j}{dx^j}\left(e^{-x}x^j\right) \tag{24}$$

Where A_k is described as:

$$A_k = \frac{1}{L_j'(x_k)}\int_0^{\infty} \frac{L_j(x)e^{-x}}{x - x_k} dx = \frac{(j!)^2}{x_k\left(L_j'(x_k)\right)^2}, L_j = e^x \frac{d^j}{dx^j}\left(e^{-x}x^j\right) \tag{25}$$

The weight functions $e^{-\frac{i\gamma}{3}}$, $e^{-\frac{i\gamma}{3}}$ with the residual errors are minimized. Finally, a MATHEMATICAL tool was used to compute the unknown coefficients. Fig. 4 displays the flow chart of the GWRM scheme.

5. Results and Discussion

In this section, the effect of controlling parameters on velocity $f'(\gamma)$,temperature field $\theta(\gamma)$, and entropy production (N_G) are display graphically. The parameters considered in this problem are given numerical values as follows $E_N = 2$, $Q_N = 1$, $R_N = S = \varpi_N = K_N = \delta_N = B_i = 0.1, \Pr = 0.71, \Lambda_N = 0.01,$ unless specifically stated in the graphs or tables.

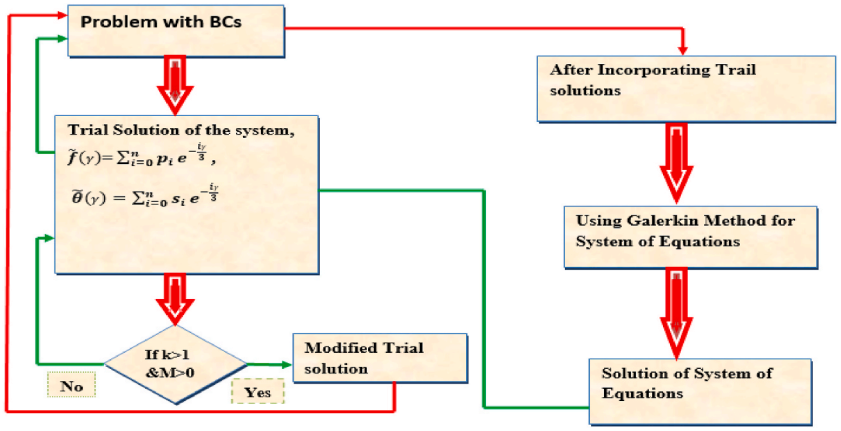

Fig. 4. The GWRM flow chart.

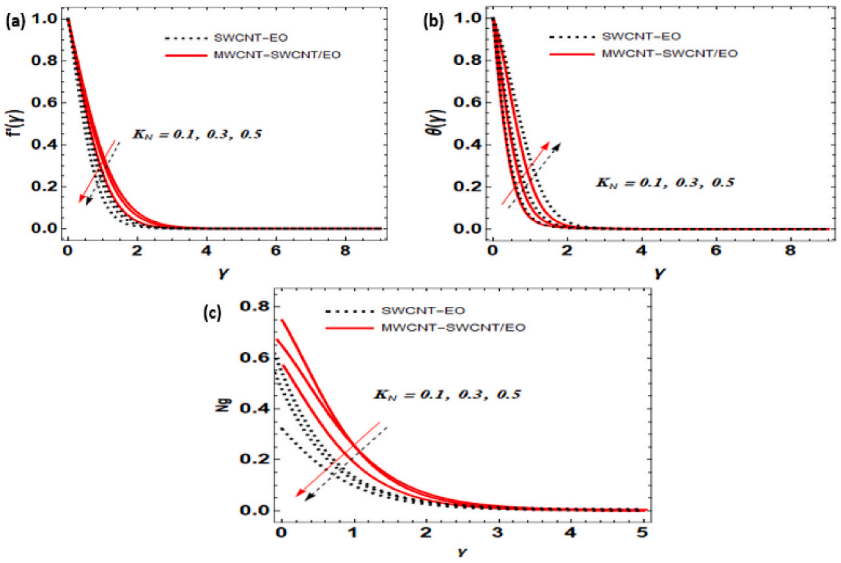

Fig. 5. Effect of K_N on $f'(\gamma)$, $\theta(\gamma)$, and N_G.

5.1. *Effect of permeability parameter* K_N *on the velocity profile for MWCNT−(SWCNT/EO) Hybrid nanofluid (HNF) and SWCNT-EO nanofluid (NF)*

The porous constraint is one of the effective methods that may significantly influence the important features of this current problem, such as fluidity, thermal energy, and entropy production. The velocity reduces when the value of the modified permeability parameter is elevated. Based on the evidence presented in Fig. 3a, it can be deduced that an increase in the permeability of a porous medium leads to a decrease in the fluid velocity that passes through the porous material. As a result of this, the motion is slowed down, and resistance is created near the wall surface. An increase in porosity means a substantial increase in the flowing pores, which in turn opposes the usage of energy. The reason for this is that the flowing porous structure makes it less likely for NPs to collide. The viscous force, which also slows the flow rate, influences the buoyancy force and controls its magnitude. On the other hand, Fig. 3b reveals the opposite response: an increase in permeability term leads to an increase in fluid temperature. The viscosity of the carbon nanofluids is suppressed as the free flow that conducts NF is assisted. Even though the thermal distribution is dominated by SWCNT/EO rather than MWCNT-SWCNT/EO, the reverse pattern can be seen for the velocity profiles. Therefore, due to the high density and viscosity of the different carbon tubes of NF, the velocity component is spread out. When the flow is slower, there is a greater chance of absorbing heat from the surface, which heats the flow and leads to higher irreversibility. From Fig. 3c, it can be deduced that an increase in the permeability of a porous medium leads to a decrease in the fluid velocity that passes through the porous material. Therefore, the

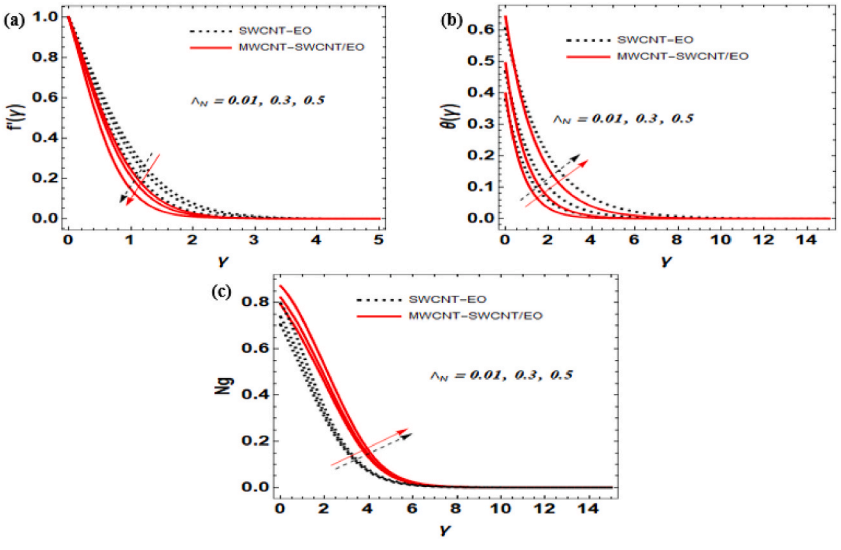

Fig. 6. Effect of Λ_N on $f'(\gamma)$, $\theta(\gamma)$ and N_G.

motion is slowed down, and resistance is created near the wall surface. This behavior is caused by the existence of a large temperature difference at the surface, which makes entropy production enhanced. Consequently, prudent choice of the permeability of the porous medium will provide an efficient approach for adjusting the coating flow properties in manufacturing sectors. Also, the porous medium will make it easier for the carbon NPs to move around, which will help to reduce the friction at the stretched surface.

5.2. *Influence of Deborah numberon the velocity profileforMWCNT− (SWCNT/EO) and SWCNT-EO nanofluid (NF)*

The influence of Λ_N on the velocity profile is depicted in Fig. 6a, which shows the flow curves of viscoelastic liquid behave in a decreasing pattern. The Λ_N dependent on the elasticity material as well as its viscosity. As (Λ_N) increases, the elastic characteristics improve, causing greater resistance to be generated by a fluid's motion and decrease the velocity distribution. Based on this finding, it was observed that the velocity profile of SWCNT-Engine oil NF is lower than that of MWCNT−(SWCNT/EO) HNF. However, the reverse pattern of behavior is observed for temperature distributions. The amount of friction that exists between nanoparticles rises, and therefore the temperature distribution rate of HNF Maxwell fluid increases as displayed in Fig. 5b.it was shown that the temperature distribution rate of SWCNT-Engine oil NF is higher than that of MWCNT−(SWCNT/EO) HNF. In Fig. 5c, we can observe the physical performance of the entropy production for the (Λ_N). It reveals a diminution in N_G close to the surface, whereas a slight increase is seen at a distance from it. When values of (Λ_N) are raised, the graphs act inversely. it was observed that the temperature distribution rate of SWCNT-Engine oil NF is higher than that of MWCNT−SWCNT/EO HNF. Therefore, this causes the production of entropy to upsurge which makes the particles move in different ways.

5.3. *Effect of velocity slip* $(\mathrm{K_N})$ *on the velocity* $\mathrm{f}'(\gamma)$*, temperature distribution* $\theta(\gamma)$*, and entropy generation* $(\mathrm{N_G})$ *for MWCNT−(SWCNT/EO) Hybrid nanofluid (HNF) and SWCNT-EO nanofluid (NF)*

This study investigates the impact of (ϖ_N) generated from boundary conditions on the flow of $f'(\gamma)$, $\theta(\gamma)$ *and*N_G as shown inFig. 7a, b, and c respectively. When the velocity slip parameter is enhanced, the fluid's viscosity increases, and the flow rate slows down. According to the results, the moving boundary sheet improves the thermal performance of MWCNT-SWCNT. The stretching velocity helps the fluid particle thermal transmission better and raises the efficiency of the carbon nanotube heat conduction. Therefore, the velocity flow slows down since the surface becomes more slippery and lubricated, and the stretching pull is only partially transferred to the fluid. On the contrary, (K_N) has the opposite effect on thermal distribution, which causes the temperature of the NF edge layer to rise.Fig. 7b shows that SWCNT/EO has a much greater effect on the temperature than MWCNT- SWCNT/EO. It is anticipated that MWCNT-SWCNT/EO will have a temperature that is a lesser effect than that of SWCNT-EO. This is because the hybrid nanofluid has a lower viscosity than the conventional nanofluid. In addition, Fig. 7c shows the (K_N) on entropy generation. A decreasing trend in entropy production can be observed with greater slip values. Entropy production exhibits high values near the sheet under no-slip conditions since these conditions lead to greater flow and thermal differences. Due to the massive velocity and temperature gradients that are caused by no-slip situations, entropy production reaches its highest values in the region near the stretching surface. In the context of the present research, the slip condition at velocity was applied, which was the cause of entropy production showing a steady decrease close to the stretching walls.

5.4. *Effect of solid volume fraction*(φ_2) *on the velocity* $\mathrm{f}'(\gamma)$*, temperature distribution* $\theta(\gamma)$*, and entropy generation* $(\mathrm{N_G})$ *for MWCNT−(SWCNT/EO) Hybrid nanofluid (HNF) and SWCNT-EO nanofluid (NF)*

Fig. 8a, b, and c show the effect ofsolid volume fraction (φ_2) on $\mathrm{f}'(\gamma)$, $\theta(\gamma)$ and $\mathrm{N_G}$. FromFig. 8a, an increase φ_2 parameter reduces

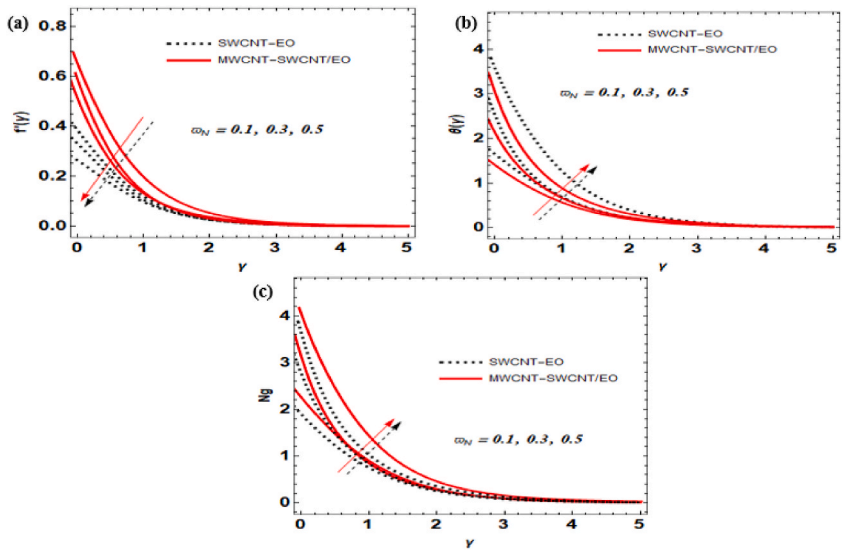

Fig. 7. Effect of K_N on $f'(\gamma)$, $\theta(\gamma)$ and N_G.

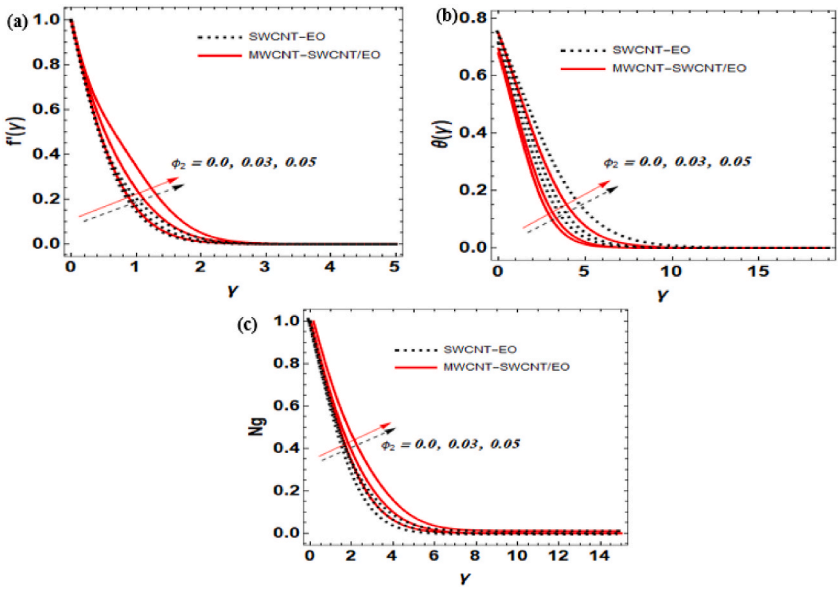

Fig. 8. Effect of φ_2 on $f'(\gamma)$, $\theta(\gamma)$ and N_G.

the flow velocity distribution while encouraging the temperature distribution. However, due to the low thermal boundary viscosity film, the dimensional aspects of motion magnitudes are reduced all over the region. This is because the film enables rapid heat dissipation out of the system, which in turn decreases the amount of heat that is stored inside the fluid flow (as seen inFig. 8a). Also, its flowability decreases when the fractional size of NPs improves due to the extra stress. The solid volume fraction promotes the HNF over the single nanofluid. As can be seen from the flow patterns, nanofluid material has excellent convective and conductive heat transfer coefficients. Therefore, nanofluids are the thermal transport factors that are driving most of the key industrial and technological improvements at this present time. Also, nanomaterials are responsible for an increase in the temperature field, as seen in Fig. 8b. Physically, in a perfect solution, the solid volume fraction corresponds with the volume percentage of the HNF; in consequence, the volume of the solution is equal to the volume of the entire carbon nanotube constituents. In the above-mentioned BF, the speed of the walls of both multiple and single carbon nanotubes slows down molecular diffusion. This means that there are fewer collisions amongNPs and the flowing boundless medium. Experiments have shown that the smallest possible size of nano molecules may be used to produce the lowest possible temperature distributions. For increasing φ_2 values, an increasing trend in entropy production is observed. Entropy generation is defined as the generation of disorder in an irreversible process. This determines the amount of energy wasted, which results in a decrease in the performance of technical systems. As can be observed, increasing the values of the parameters causes a higher level of energy loss close to the stretching plate, which leads to the system being irreversible. Because the

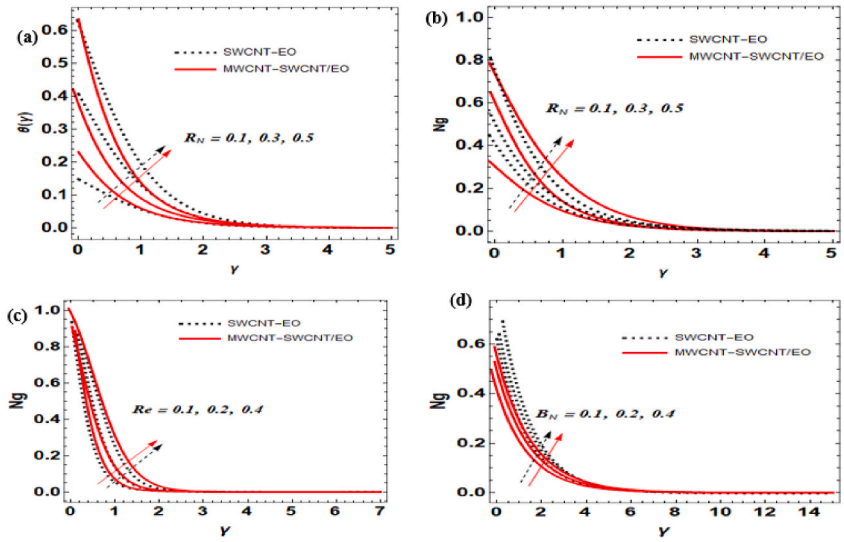

Fig. 9. Effect of $R_N B_N$ *and Re* on $\theta(\gamma)$ and N_G.

liquid thermodynamic equilibrium is increasing and consistently toward the free field, the irreversibility caused by molecular diffusivity, resistance, and heat transfer decreases from the stretching surface. The creation of entropy proceeds to reduce until a stable thermodynamic equilibrium is achieved, and thermal dissipation gradually decreases. By increasing this value, it is possible to emulate the loading of the nanoparticle in the fluid that is moving inside the enclosure. As the φ_2 increases, entropy production increases along the stretching walls. This behavior is observed in Fig. 8c.

5.5. *Effect of Thermal radiation* R_N, *Brinkmann number* (B_N), *eynolds number (Re)* and *on the temperature distribution* $\theta(\gamma)$, *and entropy generation* (N_G) *for MWCNT−(SWCNT/EO) Hybrid nanofluid (HNF) and SWCNT-EO nanofluid (NF)*

Radiation is produced when solar light re-radiated by earth surface and atmosphere after being absorbed. Also, the motion of molecules inside a substance gives rise to a specific kind of electromagnetic radiation called thermal radiation. When an electric current flows through a material, it creates electromagnetic radiation, which in turn creates a heat radiation. The effect of solar radiation on $f'(\gamma)$, $\theta(\gamma)$ and N_G is displayed in Fig. 9(a,and b). A greater amount of heat is required to be transferred to the flow because of the heat generated by thermal radiation. Radiation can be generated at a greater distance, leading to a high-temperature boundary layer flow. The radiative flux promoted the nano-polymeric wave, which provided additional thermal energy to the process even though the thermal radiation parameter had been increased. The radiative transport is less impacted by thermal boundary layer thickening and buoyant force than conduction transport. The thermal boundary layer becomes stronger as a result of the elevated temperature. Fig. 9(b)shows the Nr effect on entropy generation. The entropy of the MWCNT-(SWCNT/EO) Hybrid nanofluid (HNF) increases more than that of the SWCNT-EO Nanofluid (NF). This effect is caused by the increase in kinetic energy of random atom movements. The effect of Brinkmann number (B_N), Reynolds number (Re)on $f'(\gamma)$, $\theta(\gamma)$ and N_G is displayed in Fig. 9(c) and (d) respectively. The production of entropy serves as the model for irreversible energy losses, and the objective of the research is to identify ways to reduce the rate at which it happens. To achieve this goal, we must first identify the elements that tend to increase the entropy rate and then work to reduce that rate as much as possible. Fig. 9(c)depicts how inertial forces help the systems improve, which enables the system of entropy production to grow as the Re increases. The particles that are contained within the HNF have a significant amount of kinetic energy, which allows them to accelerate at a quicker speed with higher value of Re. The combined performance of the particles in the hybrid nanofluid caused it to create a greater entropy rate than the nanofluid. The investigation of the influence of the Br is interesting because it indicates the rate between the temperature that is created by viscous dissipation and the temperature that is transmitted by molecular conduction. Fig. 9(d)demonstrates that the Brinkman number reflects the amount of entropy that is generated by the system. Viscous dissipation is shown to be more important than any other factor in creating heat.

5.6. *Effect of thermal relaxation time* (δ_N) *Eckert number Ec and eat generation* (Q_N), *on the temperature distribution* $\theta(\gamma)$, *and entropy generation* (N_G) *for MWCNT− (SWCNT/EO) Hybrid nanofluid (HNF) and SWCNT-EO nanofluid (NF)*

Fig. 10a demonstrates how the δ_N influences the maxwell HNF thermal profile. Increasing valueof δ_N signifying a drop in temperature.This occurs since heat waves in NF require more time to transmit to achieve a larger amount of thermal relaxation time scale, and the transformation of heat within a material occurs more slowly. Therefore, the heat distribution of the Maxwell MWCNT-SWCNT/EO HNF exhibits a decreasing trend (see Fig. 10a).Fig. 10b show the impact of δ_N on entropy generation for MWCNT−SWCNT/EO HNF and SWCNT-EO NF. The entropy production is dramatically accelerated by an increasing value of δ_N.The physical reason for the increase in the size of the δ_N is that, the thermal transport rate in the non-Newtonian viscoelastic liquid regime is rising at a greater rate.

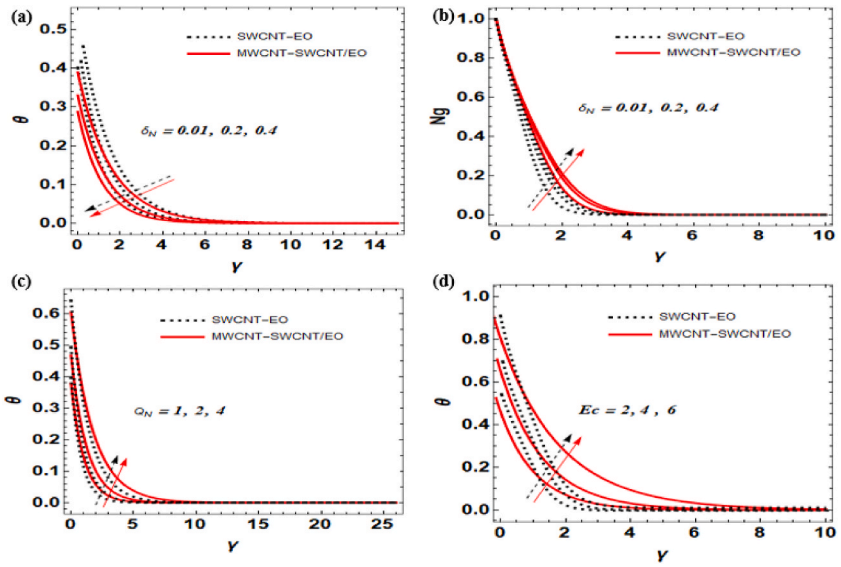

Fig. 10. Effect of δ_N, Ec, and Q_N on $\theta(\gamma)$ and N_G.

The temperature of the Maxwell MWCNT-(SWCNT/EO) HNF is influenced by the Q_N as seen in Fig. 10c.The heat is generated by transferring the thermal energy into the flow, which enables the thermal distribution of the flow to increase. Also,thefinding shows that the terms are stimulated by the heat production term in the temperature equation for the Maxwell HNF. The Q_N in the energy equation are set to increase the amount of heat creation inside the Maxwell MWCNT-(SWCNT/EO) HNF. This causes the thermal distribution to rise by a large amount of Q_N.Therefore, as Q_N emit radiation and produce greater amounts of heat in the fluid, the thermal distributionof the Maxwell MWCNT-(SWCNT/EO) HNF gradually become more intense. The impact of Eckert number (Ec) is displayed in Fig. 10d. However, the system will generate heat from all the energy lost by viscous dissipation, as is common knowledge. When the internal energy of the nanofluid is greater than its kinetic energy, which causes an increase in the thermal energy of the nanofluid, the convective movement of the nanofluid becomes more significant. Fig. 10d illustrates this effectively, showing how rising temperatures are correlated with increasing values of the Eckert number. Even relatively low values of the Eckert number are capable of having a sizeable impact on the temperature distribution. The dissipation effects cause a lot of heat to be created inside the regime, and this is shown by the fact that the temperature rises steadily throughout the stream term.

5.7. *Relative thermal transport rate (Nusselt number (Nu_x))inMWCNT−SWCNT/EO hybrid nanofluid and SWCNT-EO nanofluid*

Comparative analysis of the incorporated constraint on the temperature distribution was performed for both MWCNTs and SWCNTs. It is important to consider the effect of different aspects of the physical parameter, including the drag-force (C_f) and Nusselt number (Nu_x). This comparative percentage is displayed in Table 3. However,it was revealed that an increment of Ec rise (2, 4, 5). The relative percentage of the least point is 2.4% whereas the highest value is 2.6% point. Also, from the table, it was displaced that the solar radiation rise (0.1, 0.3, 0.5), therefore, the comparative percentage of the smallest point is 2.4%, while the greatest is 2.7% point. Furthermore, it was shown that minimum and maximum relative MWCNT−SWCNT/EO Hybrid nanofluid and SWCNT-EO nanofluid are between point 2.3% and 2.7% for increasing value of δ_N (0.01, 0.2, 0.3). For increasing value of φ_2, the lowest value is 2.2% point and highest value is2.7%. The minimum relative percentage of both MWCNT−SWCNT/EO Hybrid nanofluid and SWCNT-EO nanofluid heat transfer rate varied from 2.2% to 2.6% for increasing value of B_i. In summary, all the physical parameters favor the heat transfer rate.

To verify the accuracy of our technique, we compare our current results for Nusselt number $(Nu_{\bar{x}})$ to the previous study in Table 4. Therefore, present works is comparable and display a great accurate outcome.

6. Closing remarks

The theoretical research on solar-powered ships utilizing Maxwell MWCNT(SWCNT/EO) Hybrid nanofluid (HNF) and SWCNT-EO nanofluid (NF) in PTSC via a stretched sheet was examined. A computational model was developed, and the Catteneo–Chirstov impacts were applied to analyze the heat transmission process. The utilization of a Maxwell NNF model was also discussed. The research covered thermophysical properties, thermodynamics, and solar radiation across a stretched surface, with applications in photovoltaic cells, solar energy plates, solar lamps, and solar water pumps. The novel findings of the study are as follows:

- The velocity slip parameter decreases both speed and entropy but has the reverse impact on the temperature profiles.
- The volume fraction enhances fluidity, while the permeability parameter and the Deborah number delay the fluidity.
- The relaxation time parameter works against temperature distribution, while the permeability parameter and Deborah number act in favor of temperature distribution.
- The hybrid nanofluid of MWCNT-SWCNT/EO generates a higher level of thermal radiative improvement than the conventional SWCNT-EO nanofluid.
- The thermal efficiency of MWCNT- SWCNT/EO HNF performs better than SWCNT-EO NF, with a relative improvement ranging from 2.4% to 2.7%.

Table 3
Value of skin resistance (C_f) and wall heat gradient (Nu_x) for Pr = 7.38

Ec	R_N	δ_N	φ_2	B_i	C_f SWCNT-EO	C_f MWCNT – SWCNT/EO	Nu_x SWCNT-EO	Nu_x MWCNT – SWCNT/EO	Relative, $\frac{Nu_{\mathrm{MWCNT-SWCNT/EO}} - Nu_{\mathrm{SWCNT/EO}}}{Nu_{\mathrm{MWCNT}}}$, $\times 100$
2	0.1	0.01	0.02	0.1	5.4422	6.6777	4.5024	4.6123	2.4%
4					5.4422	6.6777	4.3531	4.4689	2.5%
6					5.4422	6.6777	4.3049	4.4229	2.6%
	0.1				5.3111	6.1100	4.4030	4.5140	2.4%
	0.3				5.3111	6.1100	4.4299	4.6531	2.6%
	0.5				5.3111	6.1100	4.5740	4.7049	2.7%
		0.01			5.2437	6.3755	4.4639	4.5679	2.3%
		0.2			5.5412	6.6442	4.5030	4.6119	2.4%
		0.4			5.6459	6.7197	4.5480	4.6650	2.5%
			0.02		–	6.3552		4.4039	2.2%
			0.03		–	6.4467		4.4658	2.4%
			0.05		–	6.6971		4.5029	2.7%
				0.1	5.4812	6.7373	4.4570	4.5581	2.2%
				0.2	5.5215	6.8352	4.5025	4.6136	2.4%
				0.4	5.6970	6.8913	4.5569	4.6802	2.6%

Table 4
Comparison of LSN (Sh_x) for varying value of Prandtl number (Pr).

Pr	0.72	1.0	3.0	7.0	10
Current result	0.80863135	1.00000000	1.92368259	3.07225021	3.72067390
The results of [75]	0.8086	1.0000	1.9237	3.0723	3.7207
The results of [76]	0.80876122	1.00000000	1.92357431	3.07314679	3.72055436
The results of [77]	0.8086	1.0000	1.9236	3.0723	3.7006
The results of [78]	0.80876181	1.00000000	1.92357420	3.07314651	3.72055429

- Parameters such as the Brinkman number, Reynolds number, radiative flux, relaxation time, Eckert number, and heat generation control the entropy generation.
- The Galerkin Weighted Residual Method establishes a high level of potential, accuracy, and convergence to model the flow of Maxwell MWCNT-SWCNT/EO Hybrid nanofluid and SWCNT-EO nanofluid (NF).
- The findings of this study conform to previous research published in the past, as shown in Table 4.

Based on these findings, it can be concluded that the utilization of Maxwell MWCNT(SWCNT/EO) Hybrid nanofluid (HNF) and SWCNT-EO nanofluid (NF) in PTSC via a stretched sheet can significantly improve the thermal efficiency of solar-powered ships. The use of hybrid nanofluid generates a higher level of thermal radiative improvement than conventional nanofluids, and the Galerkin Weighted Residual Method provides a highly accurate and convergent model for studying the flow. The findings also demonstrate the importance of specific parameters such as volume fraction, permeability, Deborah number, relaxation time, and heat generation in controlling the entropy generation. The relative improvement in thermal efficiency observed in this study could lead to significant cost savings and environmental benefits in the design and operation of solar-powered ships.

Final outcomes and future direction

The present study provides valuable insights into the use of hybrid nanofluid in solar-powered ships. However, there is still room for further research to explore the potential of this technology in practical applications. Future studies could investigate the impact of different parameters on the thermal efficiency of solar-powered ships, such as the effect of changing the size, shape, and material of the stretched sheet. Additionally, further experimentation could be conducted to validate the theoretical findings of this study. Finally, it is essential to consider the environmental impact of using hybrid nanofluid in solar-powered ships. Future research could investigate the environmental implications of producing, using, and disposing of this technology, and compare it to conventional methods of powering ships. Overall, the findings of this study demonstrate the potential of using hybrid nanofluid in solar-powered ships, and future research can build upon this knowledge to further optimize this technology for practical applications.

Author statement

We have incorporated the changes suggested by both the respected reviewers.

Declaration of competing interest

The authors declare that they have no known competing financial interests or personal relationships that could have appeared to influence the work reported in this paper.

Data availability

No data was used for the research described in the article.

Nomenclature

N_G	Entropy generation
α_f	Thermal diffusivity
δ_N	Relaxation time
Λ_N	Non-Newtonian Maxwell
K_N	Porous medium
Pr	Prandtl number
ϖ_N	velocity slip
S	Suction/Injection Parameter
R_N	Solar radiation parameter
Q_N	Heat generation
C_f	drag-force
Nu_x	Nusselt number
Re_x	local Reynolds number

B_N	Brinkmann number
Re	Reynolds number
T	heat fluid
ξ	thermal relaxation
P_w	slip length
ς	fluid relaxation
k_g	porousness of material
h_g	heat transport factor
b^*x	thermal charge rate
T_w	wall temperature
T_∞	ambient temperature

References

[1] O. Juszczyk, J. Juszczyk, S. Juszczyk, J. Takala, Barriers for renewable energy technologies diffusion: empirical evidence from Finland and Poland, Sustain. Energy Technol. Assessments 15 (2022) 527.
[2] A. Kumar, P. Singh, P. Raizada, C.M. Hussain, Impact of COVID-19 on greenhouse gases emissions: a critical review, Sci. Total Environ. 806 (2022), 150349.
[3] M. Mathew, Nuclear energy: a pathway towards mitigation of global warming, Prog. Nucl. Energy 143 (2022), 104080.
[4] S. Salawu, A. Obalalu, E. Fatunmbi, R. Oderinu, Thermal Prandtl-Eyring hybridized MoS2-SiO2/C3H8O2 and SiO2-C3H8O2 nanofluids for effective solar energy absorber and entropy optimization: a solar water pump implementation, J. Mol. Liq. 361 (2022), 119608.
[5] S. Salawu, A. Obalalu, M. Shamshuddin, Nonlinear solar thermal radiation efficiency and energy optimization for magnetized hybrid Prandtl–eyring nanoliquid in aircraft, Arabian J. Sci. Eng. (2022) 1–12.
[6] G. Alimonti, L. Mariani, F. Prodi, R.A. Ricci, A critical assessment of extreme events trends in times of global warming, Europ. Phys. J. Plus 137 (2022) 1–20.
[7] A. Mohammad, M. Zuhaib, I. Ashraf, An optimal home energy management system with integration of renewable energy and energy storage with home to grid capability, Int. J. Energy Res. 46 (2022) 8352–8366.
[8] L.-G. Kong, X.-L. Chen, J.-H. Gong, D.-J. Fan, B.-L. Wang, S. Li, Optimization of the hybrid solar power plants comprising photovoltaic and concentrating solar power using the butterfly algorithm, Energy Convers. Manag. 257 (2022), 115310.
[9] Y. Xu, B. Lu, C. Luo, F. Wu, X. Li, L. Zhang, Na2CO3 promoted CaO-based heat carrier for thermochemical energy storage in concentrated solar power plants, Chem. Eng. J. 435 (2022), 134852.
[10] K. Müller, S. Löw, S. Scholz, Power and thermal operations, in: Spacecraft Operations, Springer, 2022, pp. 393–416.
[11] A. Naderipour, A.R. Ramtin, A. Abdullah, M.H. Marzbali, S.A. Nowdeh, H. Kamyab, Hybrid energy system optimization with battery storage for remote area application considering loss of energy probability and economic analysis, Energy 239 (2022), 122303.
[12] G.V. Ochoa, M.V. Chamorro, O.C. Silvera, Thermo-economic and sustainability assessment of two solar organic Rankine cycles in the United States, Sustain. Energy Technol. Assessments 50 (2022), 101758.
[13] F. Shen, X. Li, Effects of fuel types and fuel sulfur content on the characteristics of particulate emissions in marine low-speed diesel engine, Environ. Sci. Pollut. Res. 27 (2020) 37229–37236.
[14] M. Sippel, D. Meyer, N. Scholliers, What about greenhouse gas emissions from students? An analysis of lifestyle and carbon footprints at the University of Applied Science in Konstanz, Germany, Carbon Manag. 9 (2018) 201–211.
[15] S. Auburger, E. Petig, E. Bahrs, Assessment of grassland as biogas feedstock in terms of production costs and greenhouse gas emissions in exemplary federal states of Germany, Biomass Bioenergy 101 (2017) 44–52.
[16] W. Sun, Y. Zhou, J. Lv, J. Wu, Assessment of multi-air emissions: case of particulate matter (dust), SO2, NOx and CO2 from iron and steel industry of China, J. Clean. Prod. 232 (2019) 350–358.
[17] Eggo Bracker, Madelaine Engelbrecht, Florian Meier, M. Palocz-Andresen, P. Pozzi, Sustainable Ship Technology, 2022. https://www.europeanfinancialreview.com/sustainable-ship-technology/.
[18] Y. Zhang, C. Yuan, Effects of vibration on output characteristics of shipboard PV modules, Regional Studies Marine Sci. 47 (2021), 101989.
[19] J.P. Kirkpatrick, An Investigation of the Effectiveness of Solar Power on Navy Surface Combatants, NAVAL POSTGRADUATE SCHOOL MONTEREY CA, 2013.
[20] U. Farooq, H. Waqas, S.E. Alhazmi, A. Alhushaybari, M. Imran, R. Sadat, et al., Numerical treatment of casson nanofluid bioconvectional flow with heat transfer due to stretching cylinder/plate: variable physical properties, Arab. J. Chem. (2023) 104589.
[21] U. Farooq, H. Waqas, R. Makki, M.R. Ali, A. Alhushaybari, T. Muhammad, M. Imran, Computation of cattaneo-christov heat and mass flux model in Williamson nanofluid flow with bioconvection and thermal radiation through a vertical slender cylinder, Case Stud. Therm. Eng. (2023) 102736.
[22] R. Mehmood, R. Tabassum, M.R. Ali, T. Muhammad, Crosswise stream of Cu-H2O nanofluid with micro rotation effects: heat transfer analysis, Nanomaterials 13 (3) (2023) 471.
[23] U. Farooq, H. Waqas, M.S. Aldhabani, N. Fatima, A. Alhushaybari, M.R. Ali, et al., Modeling and computational framework of radiative hybrid nanofluid configured by a stretching surface subject to entropy generation: using Keller box scheme, Arab. J. Chem. (2023) 104628.
[24] A.W. Hussein, M.W. Ahmed, Solar energy: solution to fuel dilemma, Int. J. Renew. Energy Technol. 2 (2014) 99–108.
[25] H. Lan, S. Wen, Y.-Y. Hong, C.Y. David, L. Zhang, Optimal sizing of hybrid PV/diesel/battery in ship power system, Appl. Energy 158 (2015) 26–34.
[26] W. Jamshed, C. Şirin, F. Selimefendigil, M. Shamshuddin, Y. Altowairqi, M.R. Eid, Thermal characterization of coolant Maxwell type nanofluid flowing in parabolic trough solar collector (PTSC) used inside solar powered ship application, Coatings 11 (2021) 1552.
[27] W. Jamshed, N.a. a.M. Nasir, S.S.P.M. Isa, R. Safdar, F. Shahzad, K.S. Nisar, M.R. Eid, A.-H. Abdel-Aty, I. Yahia, Thermal growth in solar water pump using Prandtl–Eyring hybrid nanofluid: a solar energy application, Sci. Rep. 11 (2021) 1–21.
[28] O.A. Olayemi, A.M. Obalalu, C.B. Odetunde, O.A. Ajala, Heat transfer enhancement of magnetized nanofluid flow due to a stretchable rotating disk with variable thermophysical properties effects, Europ. Phys. J. Plus 137 (2022) 1–12.
[29] M.A. Qureshi, A case study of MHD driven Prandtl-Eyring hybrid nanofluid flow over a stretching sheet with thermal jump conditions, Case Stud. Therm. Eng. 28 (2021), 101581.
[30] J. Mustafa, S. Alqaed, M. Sharifpur, Numerical study on performance of double-fluid parabolic trough solar collector occupied with hybrid non-Newtonian nanofluids: investigation of effects of helical absorber tube using deep learning, Eng. Anal. Bound. Elem. 140 (2022) 562–580.
[31] A.M. Obalalu, Chemical entropy generation and second-order slip condition on hydrodynamic Casson nanofluid flow embedded in a porous medium: a fast convergent method, J. Egyptian Math. Soci. 30 (2022) 1–25.
[32] A.M. Obalalu, L.L. Adebayo, I. Colak, A.O. Ajala, F.A. Wahaab, Entropy generation minimization on electromagnetohydrodynamic radiative Casson nanofluid flow over a melting Riga plate, Heat Transfer (2022).
[33] A. Yulaev, S. Kim, Q. Li, D.A. Westly, B.J. Roxworthy, K. Srinivasan, V.A. Aksyuk, Exceptional points in lossy media lead to deep polynomial wave penetration with spatially uniform power loss, Nat. Nanotechnol. (2022) 1–7.

[34] G. Collu, T. Bierig, A.-S. Krebs, S. Engilberge, N. Varma, R. Guixà-González, T. Sharpe, X. Deupi, V. Olieric, E. Poghosyan, Chimeric single α-helical domains as rigid fusion protein connections for protein nanotechnology and structural biology, Structure 30 (2022) 95–106. e7.
[35] P.G. Kumar, N. Thangapandian, V. Vigneswaran, S. Vinothkumar, B.M. Prasanth, S.C. Kim, Heat transfer, pressure drop, and exergy analyses of a shot-peened tube in the tube heat exchanger using Al2O3 nanofluids for solar thermal applications, Powder Technol. 401 (2022), 117299.
[36] A.S. Vijayanandan, R.S.K. Valappil, R.M. Balakrishnan, Evaluation of photothermal properties for absorption of solar energy by Co3O4 nanofluids synthesized using endophytic fungus Aspergillus nidulans, Sustain. Energy Technol. Assessments 37 (2020), 100598.
[37] L.S. Sundar, Y.T. Sintie, Z. Said, M.K. Singh, V. Punnaiah, A.C. Sousa, Energy, efficiency, economic impact, and heat transfer aspects of solar flat plate collector with Al2O3 nanofluids and wire coil with core rod inserts, Sustain. Energy Technol. Assessments 40 (2020), 100772.
[38] P.S. Reddy, P. Sreedevi, Effect of Cattaneo–Christov heat flux on heat and mass transfer characteristics of Maxwell hybrid nanofluid flow over stretching/shrinking sheet, Phys. Scripta 96 (2021), 125237.
[39] P.S. Reddy, A. Chamkha, Soret and Dufour effects on unsteady MHD heat and mass transfer from a permeable stretching sheet with thermophoresis and non-uniform heat generation/absorption, J. Appl. Fluid Mech. 9 (2016) 2443–2455.
[40] P. Sudarsana Reddy, P. Sreedevi, Entropy generation and heat transfer analysis of magnetic hybrid nanofluid inside a square cavity with thermal radiation, Europ. Phys. J. Plus 136 (2021) 1–33.
[41] S. Reddy, P. Sreedevi, A. Chamkha, Maxwell hybrid nanoliquid flow over vertical cone with Cattaneo-Christov heat flux and convective boundary condition, Authorea Preprints (2020).
[42] A.A. Hachicha, Z. Said, S. Rahman, E. Al-Sarairah, On the thermal and thermodynamic analysis of parabolic trough collector technology using industrial-grade MWCNT based nanofluid, Renew. Energy 161 (2020) 1303–1317.
[43] E. Bellos, C. Tzivanidis, Z. Said, A systematic parametric thermal analysis of nanofluid-based parabolic trough solar collectors, Sustain. Energy Technol. Assessments 39 (2020), 100714.
[44] P. Sreedevi, P.S. Reddy, Combined influence of Brownian motion and thermophoresis on Maxwell three-dimensional nanofluid flow over stretching sheet with chemical reaction and thermal radiation, J. Porous Media (2020) 23.
[45] P. Sreedevi, P.S. Reddy, Williamson Hybrid Nanofluid Flow over Swirling Cylinder with Cattaneo–Christov Heat Flux and Gyrotactic Microorganism, Waves in Random Complex Media, 2021, pp. 1–28.
[46] P. Sreedevi, P. Sudarsana Reddy, M. Sheremet, Impact of homogeneous–heterogeneous reactions on heat and mass transfer flow of Au–Eg and Ag–Eg Maxwell nanofluid past a horizontal stretched cylinder, J. Thermal Analy.Calorim. 141 (2020) 533–546.
[47] N. Biswas, M.K. Mondal, D.K. Mandal, N.K. Manna, R.S.R. Gorla, A.J. Chamkha, A narrative loom of hybrid nanofluid-filled wavy walled tilted porous enclosure imposing a partially active magnetic field, Int. J. Mech. Sci. 217 (2022), 107028.
[48] M.K. Mondal, N. Biswas, A. Datta, D.K. Mandal, N.K. Manna, Magneto-hydrothermal convective dynamics of hybrid nanofluid-packed partially cooled porous cavity: effect of half-sinusoidal heating, J. Thermal Analy.Calorim. (2023) 1–26.
[49] N. Biswas, D.K. Mandal, N.K. Manna, A.C. Benim, Enhanced energy and mass transport dynamics in a thermo-magneto-bioconvective porous system containing oxytactic bacteria and nanoparticles: cleaner energy application, Energy 263 (2023), 125775.
[50] N. Biswas, D.K. Mandal, N.K. Manna, A.C. Benim, Magneto-hydrothermal triple-convection in a W-shaped porous cavity containing oxytactic bacteria, Sci. Rep. 12 (2022), 18053.
[51] M.H. Ahmadi, M. Ghazvini, M. Sadeghzadeh, M.A. Nazari, M. Ghalandari, Utilization of hybrid nanofluids in solar energy applications: a review, Nano-Structures Nano-Objects 20 (2019), 100386.
[52] M. Gupta, V. Singh, Z. Said, Heat transfer analysis using zinc Ferrite/water (Hybrid) nanofluids in a circular tube: an experimental investigation and development of new correlations for thermophysical and heat transfer properties, Sustain. Energy Technol. Assessments 39 (2020), 100720.
[53] Y. Xuan, H. Duan, Q. Li, Enhancement of solar energy absorption using a plasmonic nanofluid based on TiO 2/Ag composite nanoparticles, RSC Adv. 4 (2014) 16206–16213.
[54] A.A. Minea, W.M. El-Maghlany, Influence of hybrid nanofluids on the performance of parabolic trough collectors in solar thermal systems: recent findings and numerical comparison, Renew. Energy 120 (2018) 350–364.
[55] F.A. Wahaab, L.L. Adebayo, A.A. Adekoya, I.G. Hakeem, B. Alqasem, A.M. Obalalu, Physiochemical properties and electromagnetic wave absorption performance of Ni0. 5Cu0. 5Fe2O4 nanoparticles at X-band frequency, J. Alloys Compd. 836 (2020), 155272.
[56] F.A. Wahaab, L.L. Adebayo, A.A. Adekoya, J.Y. Yusuf, A.M. Obalalu, A.O. Yusuff, B. Alqasem, Electromagnetic wave-induced nanofluid-oil interfacial tension reduction for enhanced oil recovery, J. Mol. Liq. 318 (2020), 114378.
[57] F.A. Wahaab, L.L. Adebayo, A. Rostami, M. Ganeson, J.Y. Yusuf, Y. Afeez, A.M. Obalalu, A. Abdulraheem, T.L. Oladosu, Microwave absorption performance of Ni0. 5Zn0. 5Fe2O4 nanoclusters at 8.2–18 GHz frequency, Indian J. Phys. 96 (2022) 723–733.
[58] L. Colla, L. Fedele, M. Scattolini, S. Bobbo, Water-based Fe2O3 nanofluid characterization: thermal conductivity and viscosity measurements and correlation, Adv. Mech. Eng. 4 (2012), 674947.
[59] D.K. Mandal, N. Biswas, N.K. Manna, R.S.R. Gorla, A.J. Chamkha, Hybrid nanofluid magnetohydrodynamic mixed convection in a novel W-shaped porous system, Int. J. Numer. Methods Heat Fluid Flow 33 (2023) 510–544.
[60] D.K. Mandal, N. Biswas, N.K. Manna, R.S.R. Gorla, A.J. Chamkha, Magneto-hydrothermal performance of hybrid nanofluid flow through a non-Darcian porous complex wavy enclosure, Eur. Phys. J. Spec. Top. 231 (2022) 2695–2712.
[61] D.K. Mandal, N. Biswas, N.K. Manna, R.S.R. Gorla, A.J. Chamkha, Role of surface undulation during mixed bioconvective nanofluid flow in porous media in presence of oxytactic bacteria and magnetic fields, Int. J. Mech. Sci. 211 (2021), 106778.
[62] D.K. Mandal, N. Biswas, N.K. Manna, D.K. Gayen, R.S.R. Gorla, A.J. Chamkha, Thermo-fluidic transport process in a novel M-shaped cavity packed with non-Darcian porous medium and hybrid nanofluid: application of artificial neural network, Ann. For. 34 (2022), 033608.
[63] A. Obalalu, O. Ajala, A. Adeosun, F. Wahaab, A. Oluwaseyi, L. Adebayo, Natural convective non-Newtonian Casson fluid flow in a porous medium with slip and temperature jump boundary conditions, Pet. Coal. 62 (2020) 1532–1545.
[64] A. Obalalu, I. Kazeem, A. Abdulrazaq, O. Ajala, A. Oluwaseyi, A. Adeosun, L. Adebayo, F. Wahaab, Numerical simulation of entropy generation for casson fluid flow through permeable walls and convective heating with thermal radiation effect, J Serb Soc Comput Mech 14 (2020) 503–519.
[65] A.M. Obalalu, Heat and mass transfer in an unsteady squeezed Casson fluid flow with novel thermophysical properties: analytical and numerical solution, Heat Transfer 50 (2021) 7988–8011.
[66] A.M. Obalalu, Performance of variable electrical field (VEF) on casson flow through an inclined annular micro-channel embedded in a porous medium: numerical solution by using spectral collocation method, Petroleum Coal 63 (2021).
[67] A.M. Obalalu, A.O. Ajala, A.O. Akindele, O.A. Oladapo, O.O. Akintayo, O.M. Jimoh, Computational study of magneto-convective non-Newtonian nanofluid slip flow over a stretching/shrinking sheet embedded in a porous medium, Comput. Math. Appl. 4 (2022) 123–128.
[68] E. Ghandourah, M. Hussain, M.A. Khadimallah, M. Alazwari, M.R. Ali, M.A. Hefni, Validity assessment of aspect ratios based on Timoshenko-beam model: Structural design, Comput. Concr. 31 (1) (2023) 1–7.
[69] O.A. Olayemi, K. Al-Farhany, A.M. Obalalu, T.F. Ajide, K.R. Adebayo, Magnetoconvection around an elliptic cylinder placed in a lid-driven square enclosure subjected to internal heat generation or absorption, Heat Transfer (2022).
[70] S.M. Hussain, W. Jamshed, V. Kumar, V. Kumar, K.S. Nisar, M.R. Eid, R. Safdar, A.-H. Abdel-Aty, I.J.E.R. Yahia, Computational Analysis of Thermal Energy Distribution of Electromagnetic Casson Nanofluid across Stretched Sheet: Shape Factor Effectiveness of Solid-Particles, 7, 2021, pp. 7460–7477.
[71] M. Madhu, N. Kishan, A.J. Chamkha, Unsteady flow of a Maxwell nanofluid over a stretching surface in the presence of magnetohydrodynamic and thermal radiation effects, Propulsion Power research 6 (2017) 31–40.
[72] A. Obalalu, H. Ahmad, S. Salawu, O. Olayemi, C. Odetunde, A. Ajala, A. Abdulraheem, Improvement of Mechanical Energy Using Thermal Efficiency of Hybrid Nanofluid on Solar Aircraft Wings: an Application of Renewable, Sustainable Energy, Waves in Random Complex Media, 2023, pp. 1–30.

[73] S. Salawu, A. Obalalu, S. Okoya, Thermal convection and solar radiation of electromagnetic actuator Cu–Al2O3/C3H8O2 and Cu–C3H8O2 hybrid nanofluids for solar collector optimization, Mater. Today Commun. 33 (2022), 104763.
[74] U. Khan, A. Zaib, A. Ishak, S. Bakar, Time-dependent Blasius–Rayleigh–Stokes flow conveying hybrid nanofluid and heat transfer induced by non-fourier heat flux and transitive magnetic field, Case Stud. Therm. Eng. (2021), 101151.
[75] A. Ishak, R. Nazar, I. Pop, Mixed convection on the stagnation point flow toward a vertical, continuously stretching sheet, J. Heat Tran. 129 (2007).
[76] S. Das, S. Chakraborty, R. Jana, O. Makinde, Entropy analysis of unsteady magneto-nanofluid flow past accelerating stretching sheet with convective boundary condition, Appl. Math. Mech. 36 (2015) 1593–1610.
[77] A. Ishak, R. Nazar, I. Pop, Boundary layer flow and heat transfer over an unsteady stretching vertical surface, Meccanica 44 (2009) 369–375.
[78] W. Jamshed, S. Uma Devi S, R. Safdar, F. Redouane, K.S. Nisar, M.R. Eid, Comprehensive analysis on copper-iron (II, III)/oxide-engine oil Casson nanofluid flowing and thermal features in parabolic trough solar collector, J. Taibah Univ. Sci. 15 (2021) 619–636.

2023-04-07

Computational study of þÿ C a t t a n e o C h r i s t o v h e a t f l u x o cylindrical surfaces using CNT hybrid nanofluids: a solar-powered ship implementation

Obalalu, Adebowale Martins

Elsevier

Obalalu AM, Salawu SO, Asif Memon M, et al., (2023) Computational study of þÿ C a t t a n e o C h r i s t o v h e a t f l u x o n c y l i n d r i c a l s u r f a c e s u s i n g C N T h y b r i d n a solar-powered ship implementation, Case Studies in Thermal Engineering, Volume 45, May 2023, Article number 102959

https://doi.org/10.1016/j.csite.2023.102959